

Supplementary Information

Theoretical Calculation on the Performance of Li_7NbO_6 and Doped Phases as Solid Electrolyte

Shihao Feng^{a,b}, Zhixing Wang^{b,c,d,e}, Guoshang Zhang^a, Pengfei Yue^a, Wengao Pan^a, Qiongqiong Lu^a, Huajun Guo^{b,c,d,e}, Xinhai Li^{b,c,d,e}, Guochun Yan^{b,c,d,e}, Jiexi Wang^{b,c,d,e,*}

^a Institute of Materials, Henan Academy of Sciences, Zhengzhou, 450046, P. R. China

^b School of Metallurgy and Environment, Central South University, Changsha, 410083, P. R. China

^c Engineering Research Center of the Ministry of Education for Advanced Battery Materials, Central South University, Changsha, 410083, P. R. China

^d Hunan Provincial Key Laboratory of Nonferrous Value-Added Metallurgy, Central South University, Changsha, 410083, P. R. China

^e National Engineering Research Centre of Advanced Energy Storage Materials, Changsha 410205, China

* Corresponding author, email address: wangjiexikeen@csu.edu.cn (J. Wang)

Table S1. Comparison of lattice parameters of Li_7NbO_6 between experiments and various functional calculations (keep two significant digits after the decimal point).

	a	b	c	volume
Experimental Value	5.39	5.92	5.38	126.94
PBE	5.60	5.88	5.61	133.78
LDA	5.60	5.88	5.61	133.81
PW91	5.60	5.89	5.60	133.72

According to Table S1, the lattice parameters of Li_7NbO_6 calculated based on PBE functional are similar to those of LDA and PW91 functional.

Note1:

According to the Materials Project, the convergence criteria for energy (EDIFF) is 0.0007 eV (Li_7NbO_6), 0.00135 eV ($\text{Li}_{12}\text{MgNb}_2\text{O}_{12}$ and $\text{Li}_{12}\text{MgNb}_2\text{O}_{12}$), 0.0027 eV ($\text{Li}_{26}\text{Nb}_2\text{W}_2\text{O}_{24}$), 0.00275 eV ($\text{Li}_{27}\text{Nb}_3\text{WO}_{24}$), 0.00555 eV ($\text{Li}_{55}\text{Nb}_7\text{WO}_{48}$) and 0.0057 eV ($\text{Li}_{58}\text{YNb}_7\text{O}_{48}$) respectively. The convergence criteria for force are set EDIFFG = EDIFF \times 10.

Table S2. Comparison of lattice parameters among experiments, PBE, PBE+vdW correction calculations (keep two significant digits after the decimal point).

	a	b	c	volume
Experimental Value	5.388	5.922	5.38	126.94
PBE	5.60	5.88	5.61	133.78
PBE+vdW correction	5.50	5.77	5.50	126.58

This work did not include van der Waals correction due to the fact that calculating the thermal stability (energy above hull) of materials based on the Materials Project Database, which requires the use of unified computational parameters and don't include van der Waals corrections. Here, the comparison with van der Waals corrections was made, and the results confirmed that the values of axis a, axis c and volume based on PBE with vdW correction are closer to the experimental values than PBE but the error of axis b is larger than PBE as shown in Table S2.

Table S3. Comparison of lattice parameters between $\text{Li}_{56}\text{Nb}_8\text{O}_{48}$ and its doped phases (keep two significant digits after the decimal point).

Configuration	a	b	c	volume
$\text{Li}_{56}\text{Nb}_8\text{O}_{48}$	10.97	12.08	10.78	1047.97
$\text{Li}_{48}\text{Mg}_4\text{Nb}_8\text{O}_{48}$	10.88	12.18	11.12	1054.39
$\text{Li}_{48}\text{Zn}_4\text{Nb}_8\text{O}_{48}$	10.94	12.13	11.10	1055.01
$\text{Li}_{52}\text{Nb}_4\text{W}_4\text{O}_{48}$	11.12	11.97	11.03	1045.90
$\text{Li}_{54}\text{Nb}_6\text{W}_2\text{O}_{48}$	11.07	11.95	11.06	1056.62
$\text{Li}_{55}\text{Nb}_7\text{WO}_{48}$	11.10	11.83	11.12	1064.26
$\text{Li}_{58}\text{YNb}_7\text{O}_{48}$	10.74	11.31	11.77	1074.24

The lattice parameters of $\text{Li}_{48}\text{Mg}_4\text{Nb}_8\text{O}_{48}$ and $\text{Li}_{48}\text{Zn}_4\text{Nb}_8\text{O}_{48}$ were obtained by building 2×2 supercell of $\text{Li}_{12}\text{MgNb}_2\text{O}_{12}$ and $\text{Li}_{12}\text{ZnNb}_2\text{O}_{12}$.

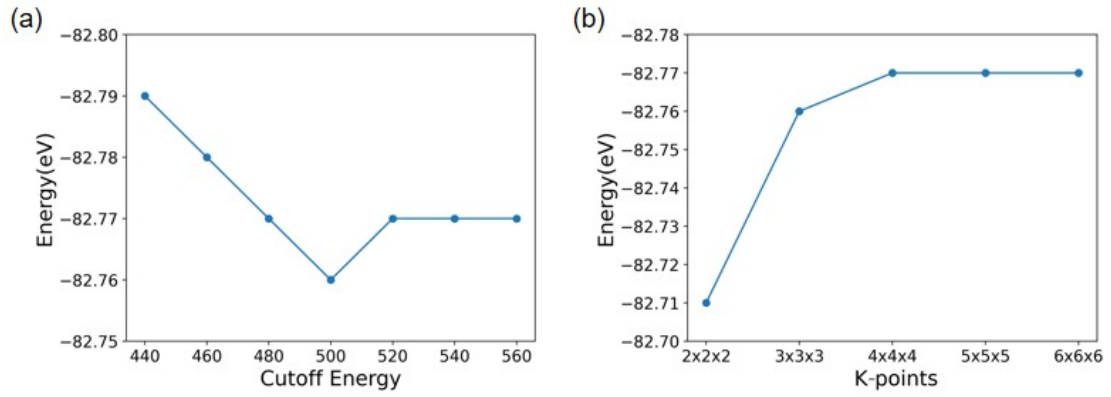


Figure S1. Based on Li_7NbO_6 cell (a) the convergence test of cutoff energy, (b) the convergence test of K-points.

The convergence tests for the cutoff energy and K-points demonstrate that the DFT energy tends to stabilize when the cutoff energy exceeds 520 eV or K-point grid density exceeds 4x4x4. The convergence tests demonstrates that the selection of the cutoff energy and K-point grid density balances computational accuracy with time cost.

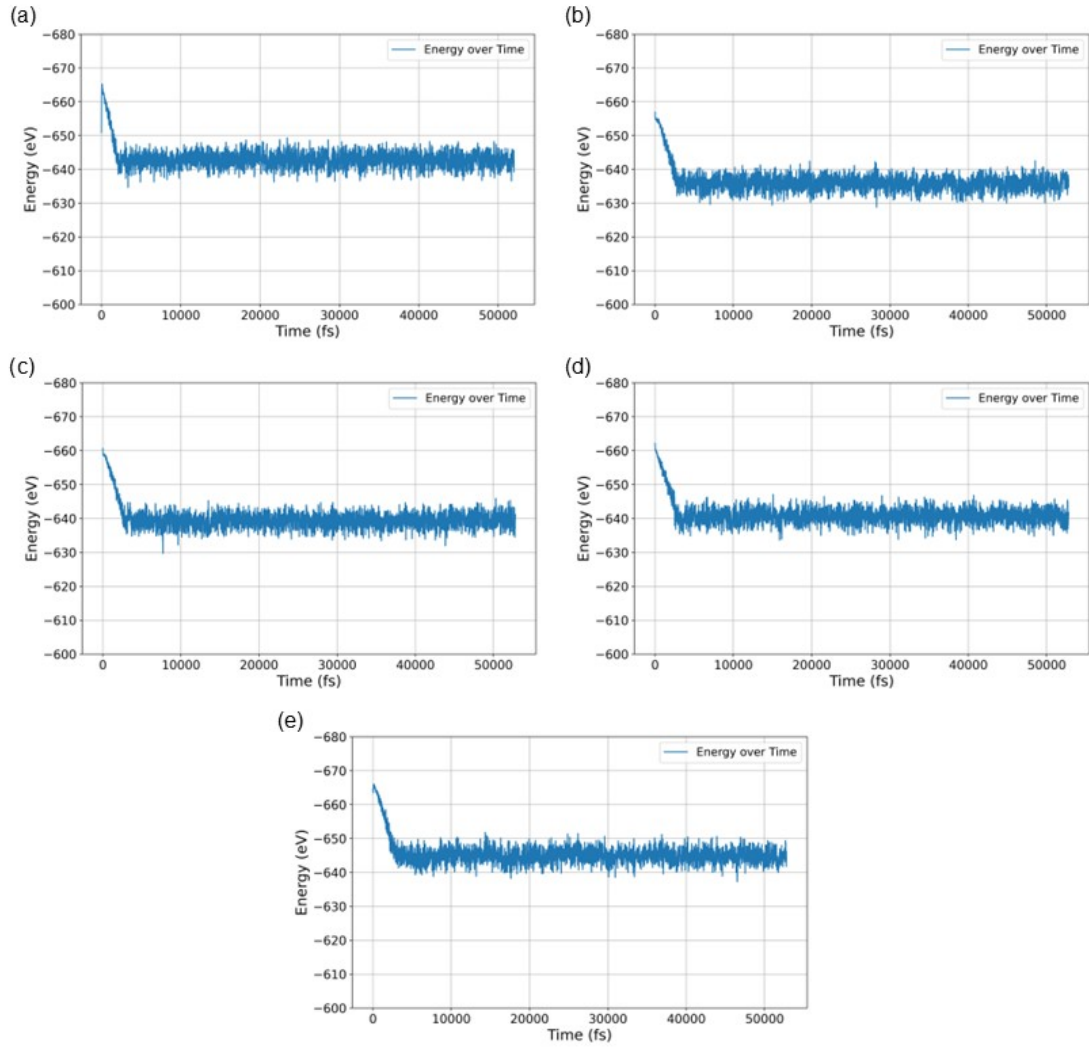


Figure S2. Variation with time of the total energy of (a) $\text{Li}_{56}\text{Nb}_8\text{O}_{48}$, (b) $\text{Li}_{52}\text{Nb}_4\text{W}_4\text{O}_{48}$, (c) $\text{Li}_{54}\text{Nb}_6\text{W}_2\text{O}_{48}$, (d) $\text{Li}_{55}\text{Nb}_7\text{WO}_{48}$, (e) $\text{Li}_{58}\text{YNb}_7\text{O}_{48}$ from preheating stage to keeping 1500 K.

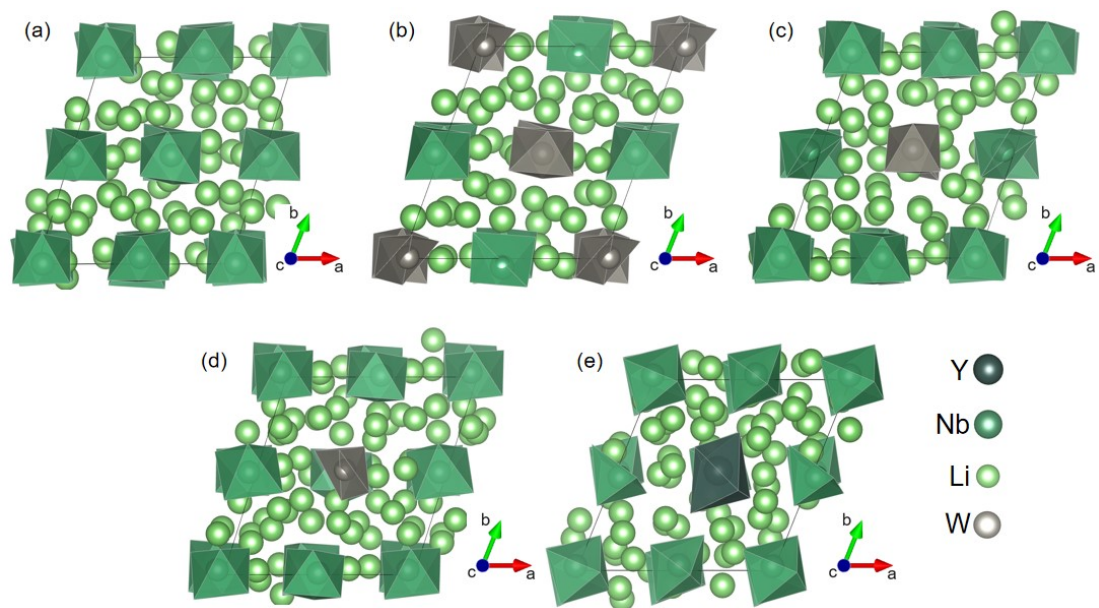


Figure S3. The structure of (a) $\text{Li}_{56}\text{Nb}_8\text{O}_{48}$, (b) $\text{Li}_{52}\text{Nb}_4\text{W}_4\text{O}_{48}$, (c) $\text{Li}_{54}\text{Nb}_6\text{W}_2\text{O}_{48}$, (d) $\text{Li}_{55}\text{Nb}_7\text{WO}_{48}$, (e) $\text{Li}_{58}\text{YNb}_7\text{O}_{48}$ after heating at 1500 K.

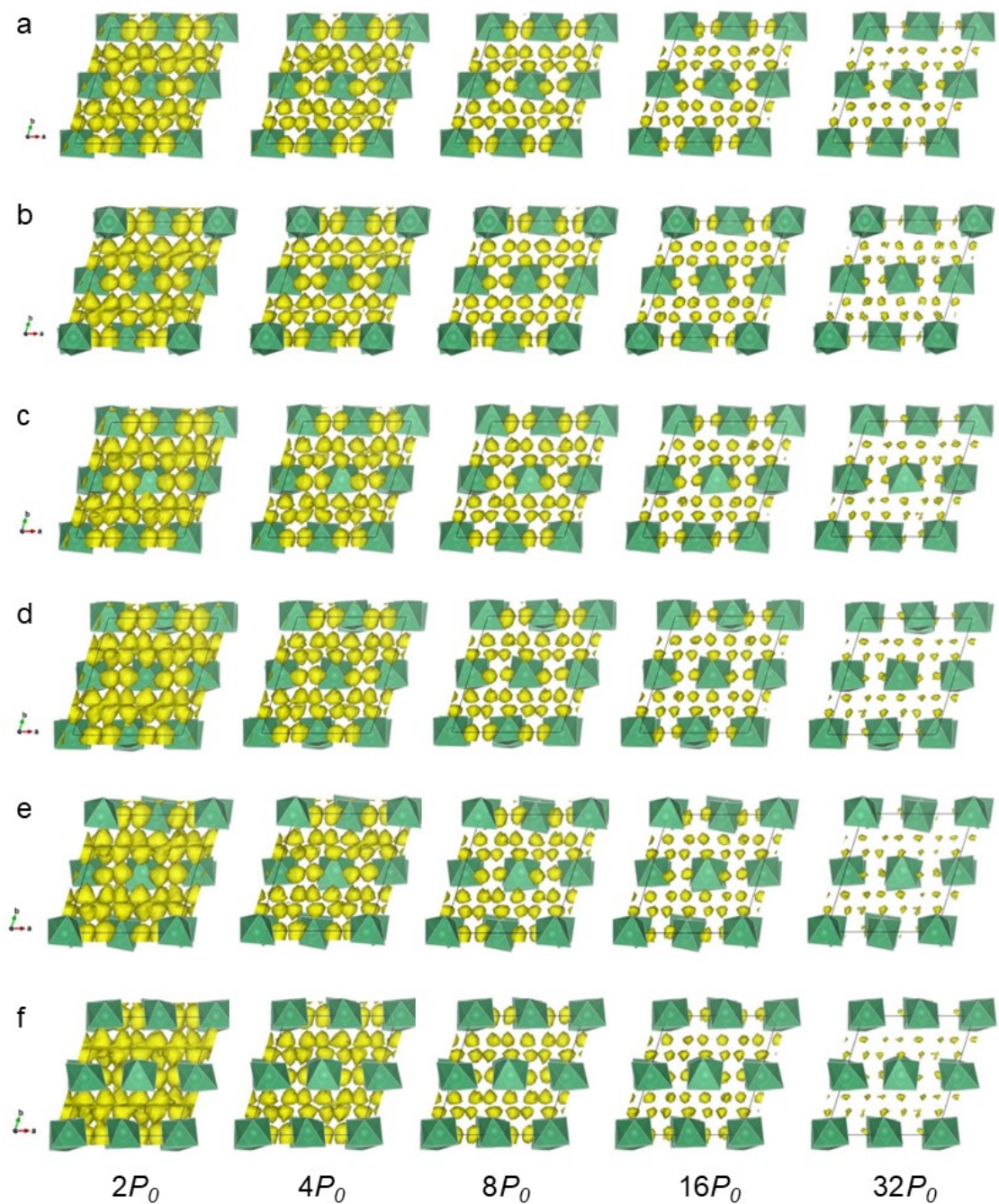


Figure S4. Lithium ions probability densities in $\text{Li}_{56}\text{Nb}_8\text{O}_{48}$. a-f, the probability densities of lithium ions are obtained from AMID simulations at 1000 K(a), 1100 K (b), 1200 K (c), 1300 K (d), 1400 K (e), 1500 K (f). Isosurfaces of the ionic probability densities are plotted at increasing isovalues ranging from $2P_0$ to $32P_0$, in which P_0 is defined as 0.0005 for each structure.

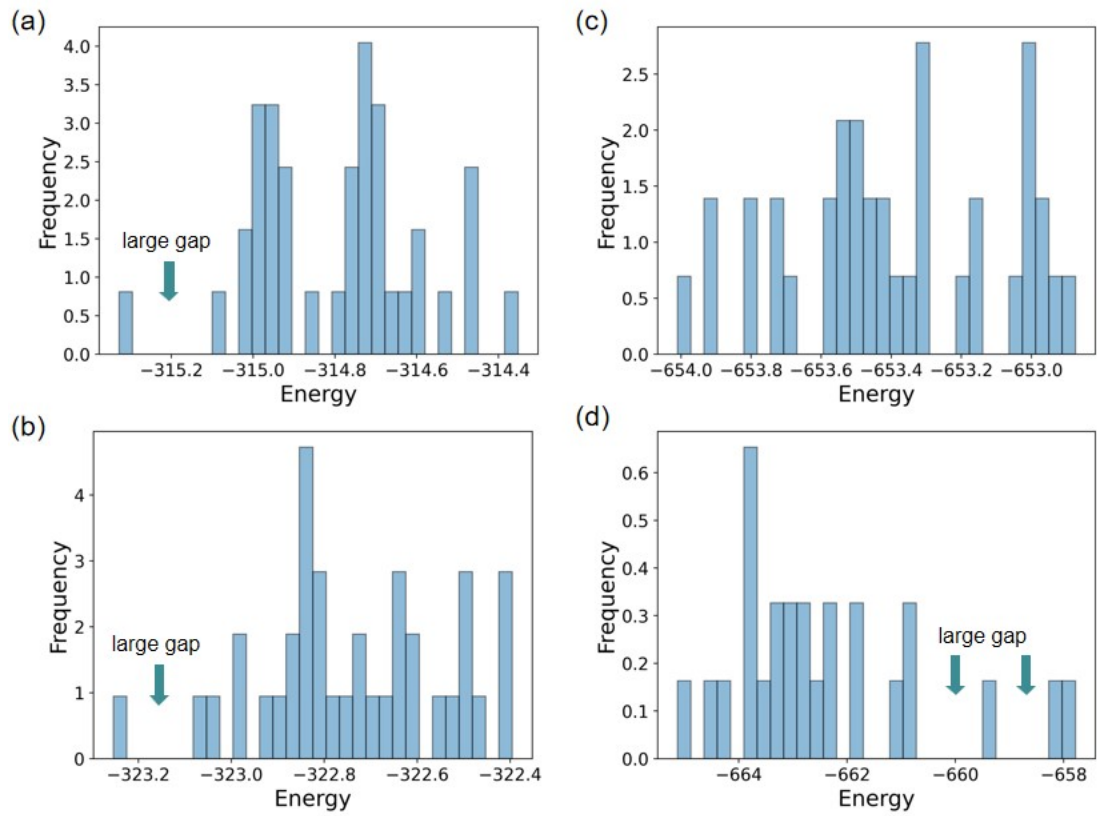


Figure S5. Frequency distribution histogram based on ordered models. (a)

$\text{Li}_{26}\text{Nb}_2\text{W}_2\text{O}_{24}$, (b) $\text{Li}_{27}\text{Nb}_3\text{WO}_{24}$, (c) $\text{Li}_{55}\text{Nb}_7\text{WO}_{48}$, (d) $\text{Li}_{58}\text{YNb}_7\text{O}_{48}$.

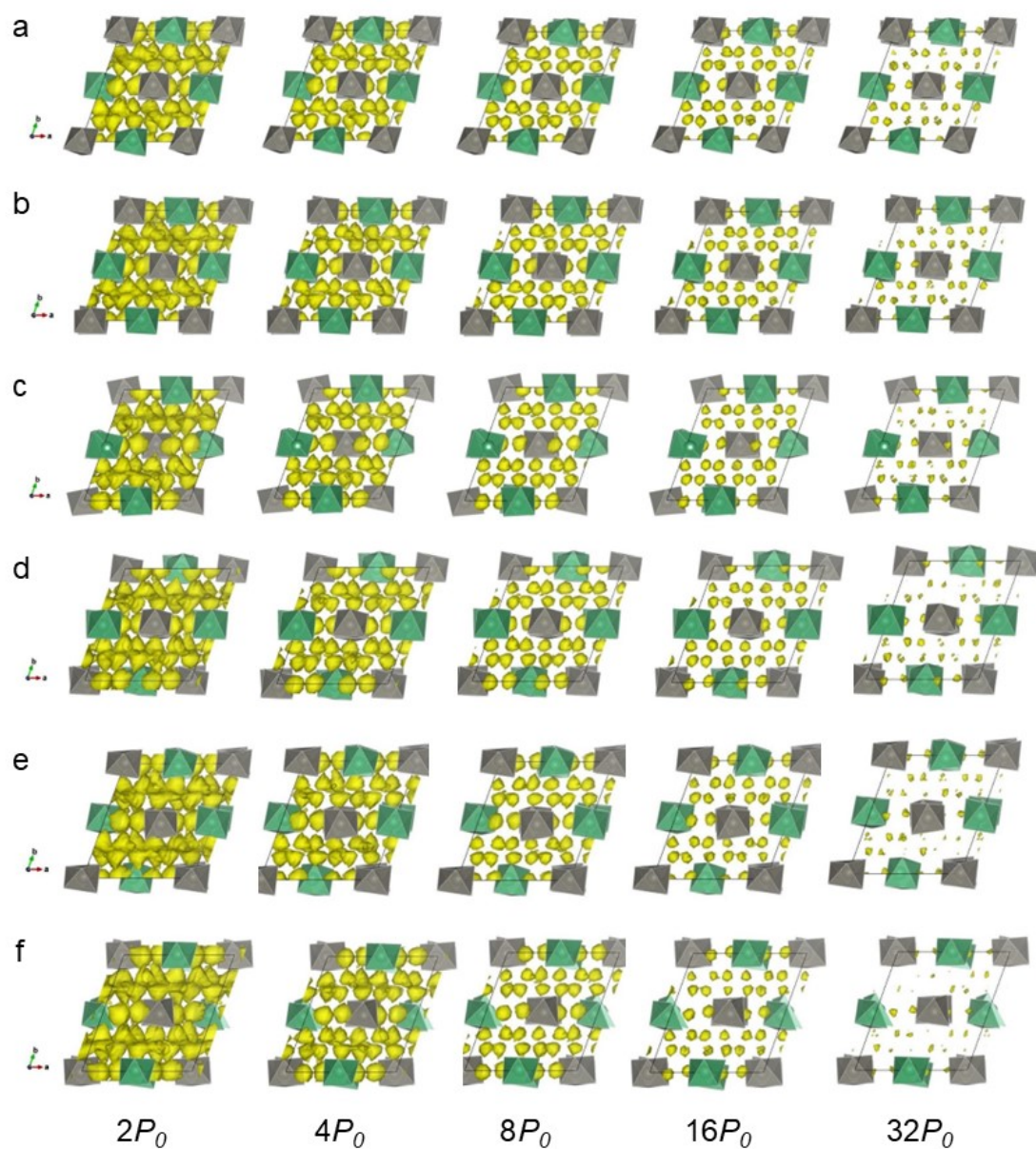


Figure S6. Lithium ions probability densities in $\text{Li}_{52}\text{Nb}_4\text{W}_4\text{O}_{48}$. a-f, the probability densities of lithium ions are obtained from AMID simulations at 1000 K(a), 1100 K (b), 1200 K (c), 1300 K (d), 1400 K (e), 1500 K (f). Isosurfaces of the ionic probability densities are plotted at increasing isovalues ranging from $2P_0$ to $32P_0$, in which P_0 is defined as 0.0005 for each structure.

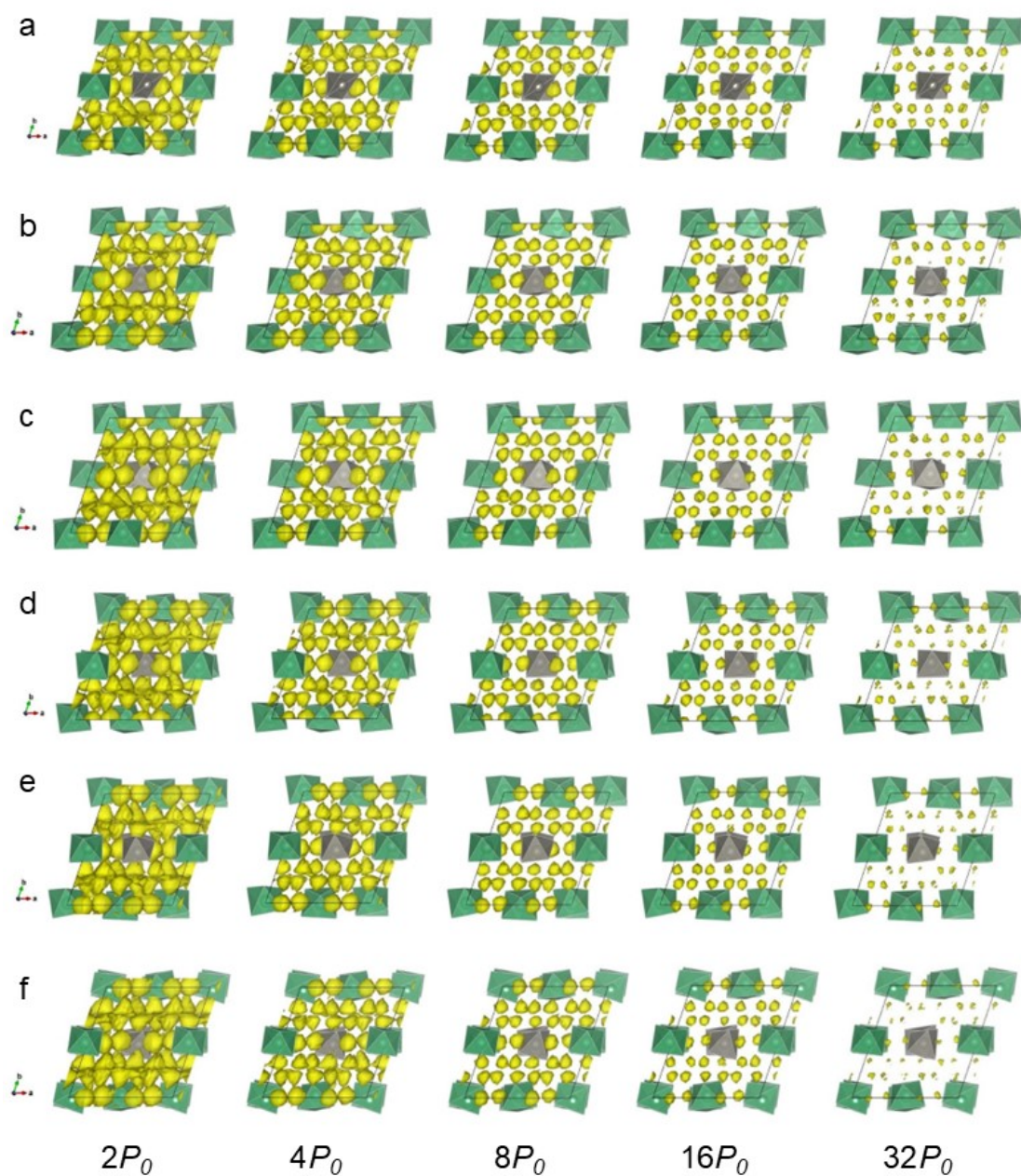


Figure S7. Lithium ions probability densities in $\text{Li}_{54}\text{Nb}_6\text{W}_2\text{O}_{48}$. a-f, the probability densities of lithium ions are obtained from AMID simulations at 1000 K(a), 1100 K (b), 1200 K (c), 1300 K (d), 1400 K (e), 1500 K (f). Isosurfaces of the ionic probability densities are plotted at increasing isovalues ranging from $2P_0$ to $32P_0$, in which P_0 is defined as 0.0005 for each structure.

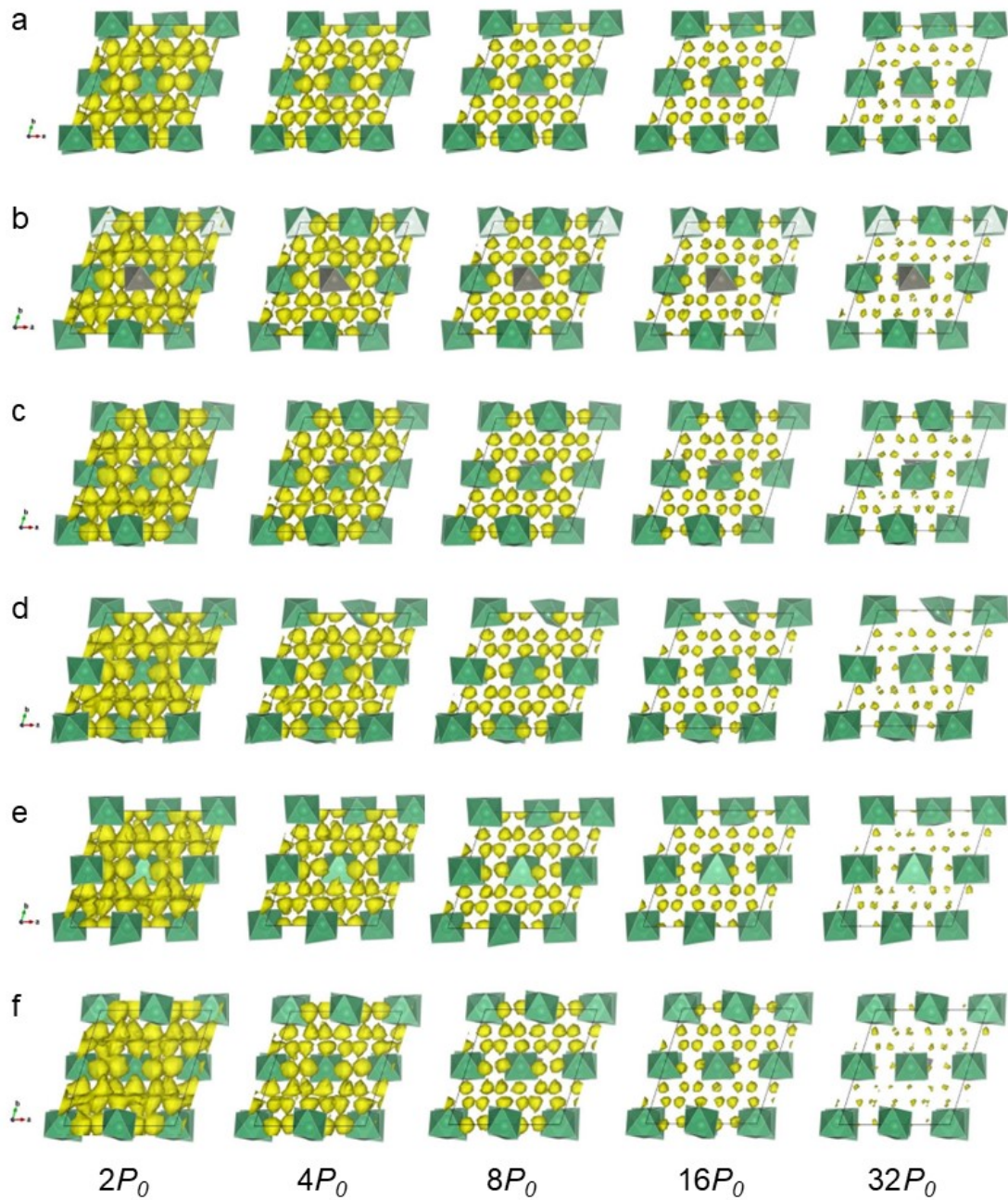


Figure S8. Lithium ions probability densities in $\text{Li}_{55}\text{Nb}_7\text{WO}_{48}$. a-f, the probability densities of lithium ions are obtained from AMID simulations at 1000 K(a), 1100 K (b), 1200 K (c), 1300 K (d), 1400 K (e), 1500 K (f). Isosurfaces of the ionic probability densities are plotted at increasing isovalues ranging from $2P_0$ to $32P_0$, in which P_0 is defined as 0.0005 for each structure.

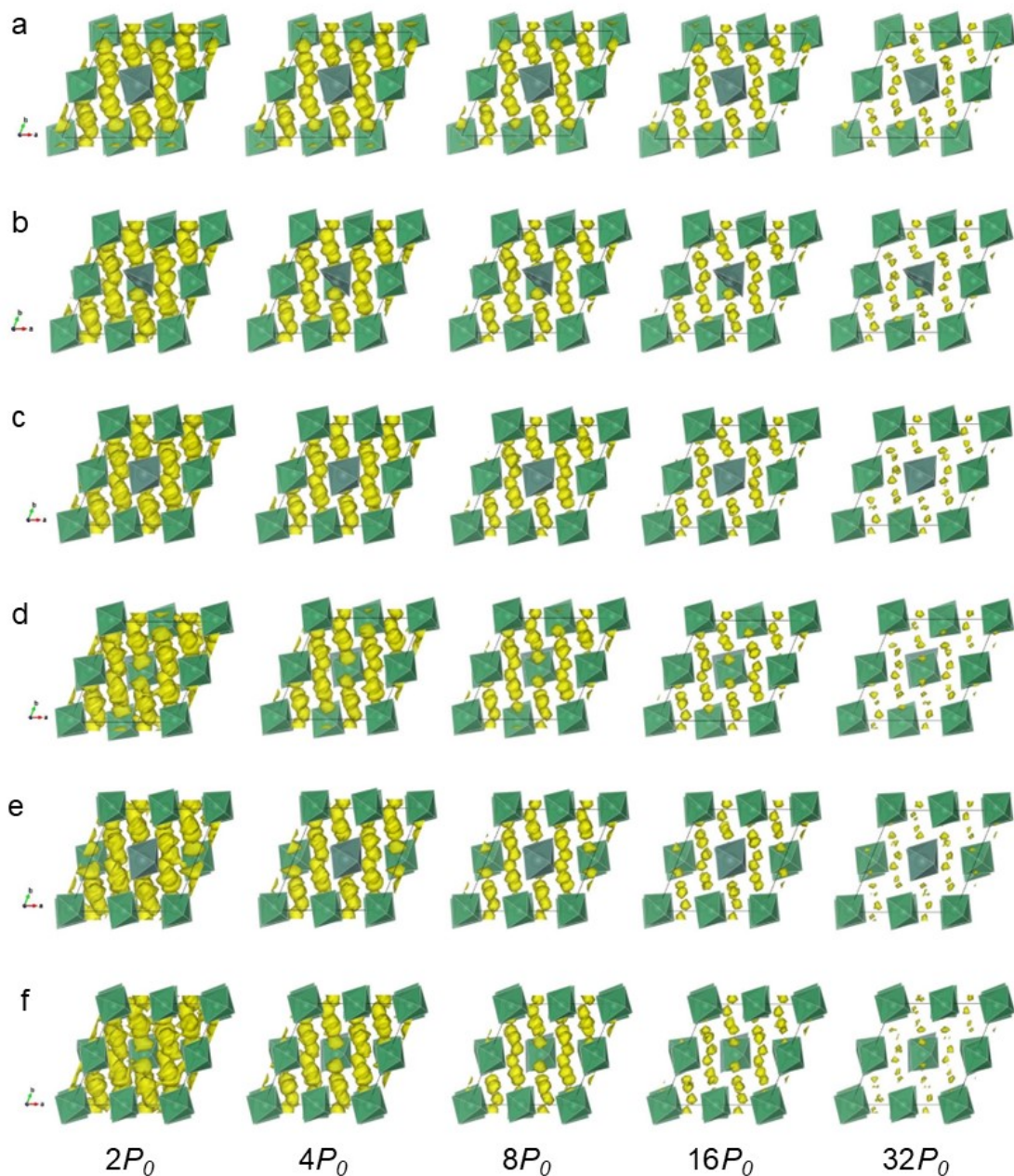


Figure S9. Lithium ions probability densities in $\text{Li}_{58}\text{YNb}_7\text{O}_{48}$. a-f, the probability densities of lithium ions are obtained from AMID simulations at 1000 K(a), 1100 K (b), 1200 K (c), 1300 K (d), 1400 K (e), 1500 K (f). Isosurfaces of the ionic probability densities are plotted at increasing isovalues ranging from $2P_0$ to $32P_0$, in which P_0 is defined as 0.0005 for each structure.